

Self-Assembly of an Octanuclear Platinum(II) Tetragonal Prism from a New Pt^{II}₄ Organometallic Star-Shaped Acceptor and Its Nitroaromatic Sensing Study

Sankarasekaran Shanmugaraju, Harshal Jadhav, Yogesh P. Patil, and Partha Sarathi Mukherjee*

Department of Inorganic and Physical Chemistry, Indian Institute of Sciences, Bangalore 560012, India

Supporting Information

ABSTRACT: [2 + 4] self-assembly of a pyrene-functionalized Pt^{II}₈ tetragonal prism (2) is achieved using a newly designed star-shaped organometallic acceptor (1) in combination with an amide-based “clip” donor (L). The propensity of this prism (2) as a selective sensor for nitroaromatics (2,4-dinitrotoluene, 1,3,5-trinitrotoluene, and picric acid), which are the chemical constituents of many commercial explosives, has been examined.

Because of its predictable directionality as well as experimental simplicity, metal–ligand coordination self-assembly has become a promising tool for constructing molecular architectures of defined shapes, sizes, and functionality.^{1,2} Three-dimensional (3D) metallacages are relatively less explored compared to two-dimensional (2D) metallacycles because of their synthetic difficulties. However, chemists have recently shown much interest in making hollow 3D-container molecules not only because of their spectacular structural features but also because of their internal nanospace capable of performing several fascinating functions.³ Among the known 3D cages, the tetragonal prism is less common in the literature because of the difficulty of making suitable building blocks. More recently, Stang et al. have synthesized a few tetragonal prisms via multicomponent self-assembly (one acceptor + two different donors).⁴ However, multicomponent self-assembly still remains underdeveloped because of the possibility of forming several entropically preferred discrete smaller polygons/polyhedra. Two-component (one acceptor + one donor) self-assembly is a widely accepted protocol.⁵ From symmetry consideration, a tetragonal prism can be designed using a planar tetrapotic building unit with complementary “clips” by [2 + 4] self-assembly.

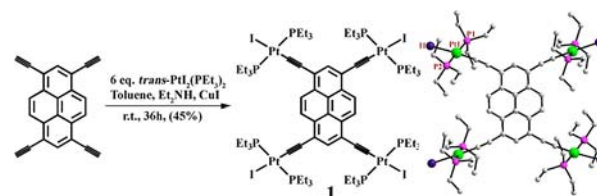
On the other hand, a selective and sensitive chemosensor for the trace detection of explosives has become a high priority for life security and environmental issues.⁶ Among the various known instrumental techniques employed to detect nitroaromatic explosives (NAEs), fluorescence-quenching-based detection has grown dramatically because of its high sensitivity and real-time monitoring with fast response time.⁷ In this context, we are currently involved in the design of suitable fluorescent receptors for the selective recognition of explosive constituents.⁸

We report here a new organometallic star-shaped pyrene-functionalized Pt₄ planar tetrapotic acceptor (1) and its self-assembly of a Pt₈ molecular tetragonal prism (2) using two

components. Prism 2 represents the first example of a platinum(II) tetragonal prism obtained via two-component self-assembly. This new prism is tested to be a quite efficient sensor for the rapid detection of NAEs.

The pyrene-based platinum(II) acceptor (1) was synthesized in moderate yield (45%) via a substitution reaction of 1,3,6,8-tetraethynylpyrene with *trans*-PtI₂(PEt₃)₂ under a nitrogen atmosphere (Scheme 1) and characterized fully (Supporting

Scheme 1. Schematic Representation of the Synthesis of Acceptor 1 (Left) and Its X-ray Crystal Structure (Right)



Information). The molecular structure of 1 was determined by single-crystal X-ray diffraction. Complex 1 was crystallized in monoclinic space group $P2_1/c$ with two formula units in an asymmetric unit. A ball-and-stick representation of the structure of 1 (Scheme 1, right) shows that it is indeed a tetrapotic platinum(II) acceptor. The coordination geometry around each Pt^{II} metal center is almost square-planar, with the I–Pt–P angles being in the range of 89.34–95.08° and the C–Pt–P angles being in the range of 84.39–91.15°. The average Pt–I bond distance is 2.64 Å.

As shown in Scheme 2, the construction of tetragonal prism 2 was accomplished in a single step. The treatment of acceptor 1 (acting as faces) with 4 equiv of AgNO₃ followed by the reaction with 2 equiv of an amide-based ditopic donor L (acting as a connector) resulted in the exclusive formation of tetragonal prism 2 in 90% yield. ³¹P{¹H} NMR spectra of 2 exhibited a sharp singlet at δ 16.16, which is upfield-shifted by 4.32 ppm from the nitrate analogue of acceptor 1 due to ligand-to-platinum(II) coordination (Figure 1). Moreover, a significant decrease in the coupling of flanking ¹⁹⁵Pt satellites (ca. $J_{Pt-P} = 1722.68$ Hz) compared to the nitrate analogue of acceptor 1 ($J_{Pt-P} = 1849.6$ Hz) is consistent with electron back-donation from platinum(II). Likewise, the appearance of simple and sharp ¹H NMR signals suggested the formation of a single prismatic cage. In the ¹H

Received: August 6, 2012

Published: November 26, 2012

Scheme 2. [2 + 4] Self-assembly of a Tetragonal Prism (2) from Acceptor 1 in Combination with an Amide-Based Ditopic Donor “Clip” (L)

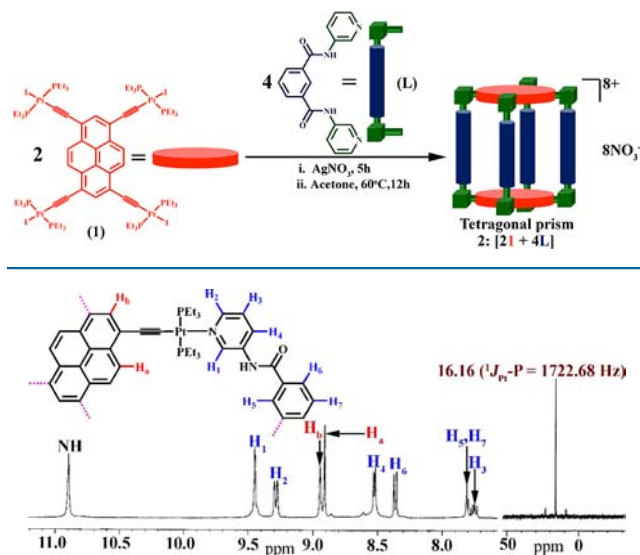


Figure 1. ^1H (left) and ^{31}P (right) NMR spectra of the tetragonal prism **2** recorded in CD_3NO_2 with the peak assignments.

NMR spectrum of prism **2**, H atoms of the pyridine rings exhibited a small downfield shift relative to uncoordinated **L** because of the loss of electron density upon coordination of pyridyl N atoms to Pt^{II} centers (Figure 1).⁸ The sharp NMR signals as well as high solubility of the resulting assembly in common organic solvents ruled out the possibility of forming any other polymeric analogue. Peaks for charged fragments at m/z 1390.27 ($[\mathbf{2} - 4\text{NO}_3^-]^{4+}$), 906.18 ($[\mathbf{2} - 6\text{NO}_3^-]^{6+}$), and 664.13 ($[\mathbf{2} - 8\text{NO}_3^-]^{8+}$) appeared in the ESI-MS spectrum of **2**. The peak due to $[\mathbf{2} - 4\text{NO}_3^-]^{4+}$ is isotopically resolved and matched with its charged state. ESI-MS results clearly demonstrate a [2 + 4] combination of the acceptor and donor in complex **2**. The only discrete geometry possible for this combination is a tetragonal prism (Supporting Information).

Attempts to obtain diffraction-quality single crystals of **2** were unsuccessful. On the basis of the mass spectrometric results, the resulting assembly is confirmed to be a [2 + 4] self-assembled prism. The optimization of the prism **2** has been done using semiempirical methods with a PM3 function to gain the structural characteristics of prism **2**. As shown in Figure 2, the energy-minimized geometry of **2** shows a tetragonal-prismatic cagelike structure with an approximate diameter of around 2.02 nm, which is comparable to the hydrodynamic radius of 1.87 nm determined by a pulsed-gradient spin-echo NMR experiment in

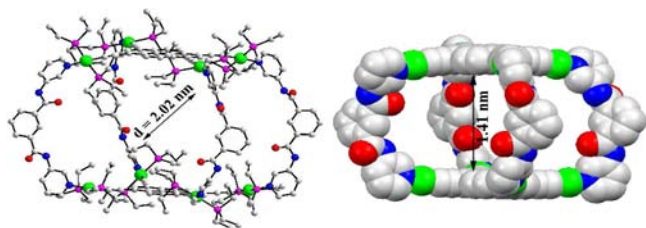


Figure 2. Ball-and-stick and CPK views of the energy-minimized structure of tetragonal prism **2**.

CD_3NO_2 solvent (Supporting Information), and the distance between the roof and floor is 1.41 nm.

Thermogravimetric analysis of the as-synthesized prism **2** indicated its high stability up to 300 °C (Supporting Information), and the surface morphology of thin films of **2** and **1** was imaged using scanning electron microscopy (SEM). As shown in Figure 3, the SEM image of a freshly made thin film of

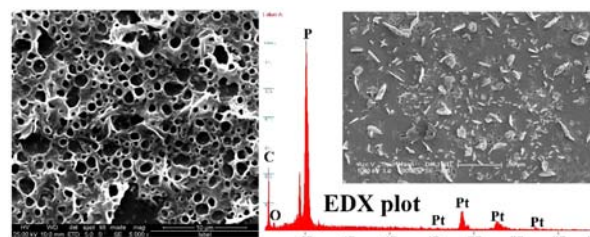


Figure 3. SEM image (left) and EDX plot (right) of prism **2** (inset right: SEM image of acceptor **1**).

prism **2** on a glass slide formed a highly porous nanoring-like pattern, whereas the thin film of **1** does not show such porosity. The chemical composition of the imaged films was characterized by energy-dispersive X-ray (EDX) spectroscopy, which indicated that the film consists of the expected elemental composition (Supporting Information).

The UV-vis absorption spectra of **1** and **2** recorded in CHCl_3 showed characteristic visible absorption bands in the ranges $\lambda = 355\text{--}482$ nm for **1** and $\lambda = 334\text{--}474$ nm for **2** ascribed to the typical $\pi\text{--}\pi^*$ and metal-to-ligand charge-transfer (CT) transitions (Supporting Information). Moreover, the linking of unsaturated ethynyl groups to the core-pyrene moiety enriches π conjugation, thereby exhibiting strong fluorescence emission characteristics. A low-temperature (77 K) emission study revealed the presence of phosphorescence due to intersystem crossing, as expected due to having many Pt^{II} centers in conjugation with the conjugated aromatic backbone (Supporting Information). To demonstrate the ability of **2** as a fluorescence sensor for NAEs, we first performed fluorescence quenching titration with 1,3,5-trinitrotoluene (TNT) in solution. The initial emission intensity of **2** in chloroform depleted rapidly upon the gradual addition of TNT in methanol (Figure 4). A linear Stern-Volmer relationship was obtained from the titration profile (Supporting Information), and the calculated Stern-Volmer binding constant is $K_{\text{SV}} = 9.7 \times 10^5 \text{ M}^{-1}$.

The quenching in the emission intensity of **2** is ascribed to the formation of a nonfluorescent CT complex between the π -electron-rich prism (**2**) and the electron-deficient quencher

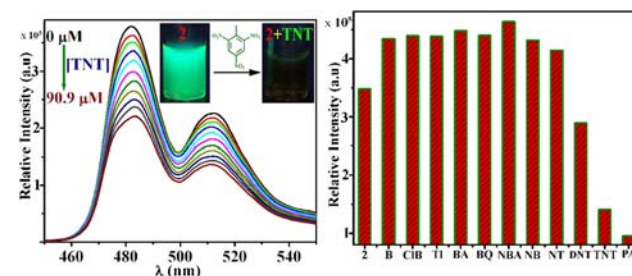


Figure 4. Reduction in the emission intensity (left) of prism **2** upon the addition of TNT (inset: visual color change of **2** upon the addition of TNT under UV light) and relative changes in the emission intensity (right) of **2** upon the addition of different quenchers.

(TNT). Formation of this CT complex is also supported by an electronic absorption study (Supporting Information). Furthermore, the time-resolved fluorescence titration study showed almost no change in the lifetime (0.8 ns) of **2** upon the gradual addition of TNT (Supporting Information) and also a sharp visual color change of **2** upon mixing with NAEs under UV light (Figure 4), which confirms that the observed fluorescence quenching follows a static-quenching mechanism via ground-state complex formation. To substantiate the role of a porous 3D supramolecular cage on the sensitivity of NAE detection, a similar fluorescence titration study of acceptor **1** with TNT was done under identical conditions (Supporting Information). The calculated Stern–Volmer binding constant from the titration profile is $K_{SV} = 1.7 \times 10^4 \text{ M}^{-1}$, which suggests that porous cage **2** is better compared to **1**. This superior sensitivity of **2** toward NAEs is ascribed to the presence of a π -electron-rich confined nanopocket, which imparts further strength to encapsulate the electron-deficient NAEs more efficiently than the fully planar molecule **1**.

Moreover, to judge the selectivity of **2** toward NAEs, we carried out the fluorescence quenching titration study with other electron-deficient/rich aromatic compounds. As shown in Figure 4, NAEs [picric acid (PA) and TNT] showed much pronounced quenching, whereas other tested compounds such as benzoquinone (BQ), benzoic acid (BA), benzene (B), and toluene (Tl) induce low response. In addition, the fluorescence study also demonstrates that prism **2** can elicit the quenching response even at parts per billion (ppb) concentration of TNT (Supporting Information), and such a level of sensitivity falls below the permissible level of TNT in drinking water.⁹

To further explore the practical use of NAE vapor sensing, we monitored the emission intensity of freshly made thin films (prepared on a quartz plate using a 1 mM chloroform solution of the sample) of **2** and **1** as a function of time, before and after exposure to saturated 2,4-dinitrotoluene (DNT) vapor on the film (DNT has a higher vapor pressure than other NAEs). The initial emission intensity of the film decreased significantly after 200 s of exposure of the film to the saturated DNT vapor at room temperature (Figure 5). The fluorescence quenching efficiency

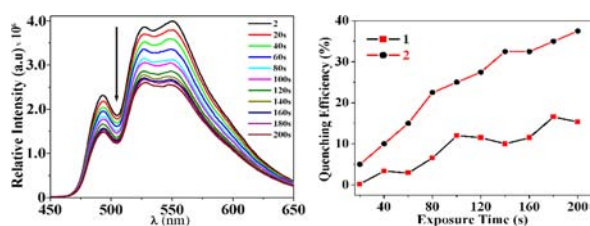


Figure 5. Time-dependent emission intensity of a thin film of prism **2** upon exposure to the saturated vapor of DNT (left) and the quenching efficiency of **1** and **2** as a function of the exposure time (right).

of **2** reached ~40%, whereas the film of **1** showed only ~13% quenching efficiency after 200 s exposure of the film (Figure 5). As anticipated, the porous nature of **2** makes it a better sensor because of the easy access of analytes to the intrinsic internal porosity of **2**.

Moreover, the thin film of **2** also showed highly reversible sensing of NAEs. After exposure of the film to a saturated vapor of DNT at room temperature for 200 s, the initial emission intensity of the film was recovered after washing with water and dried in hot air. By these treatments, the thin film quickly regains the emission intensity and thus can be reused for a significant

number of cycles (Figure S23, Supporting Information). Moreover, the efficient regaining of the initial emission intensity of **2** over a number of cycles assured the high photostability of the film for its long-time in-field application.

In conclusion, we report herein the synthesis and characterization of the very first example of a platinum(II) tetragonal prism (**2**) via the two-component directional self-assembly of a new pyrene-based planar Pt₄ acceptor **1** and an amide-based “clip” donor (**L**). The presence of π -electron-rich highly conjugated tetraethynylpyrene building units as the floor and roof makes it a potential fluorescent host for the recognition of electron-deficient NAEs in both solution and vapor phases.

■ ASSOCIATED CONTENT

Supporting Information

X-ray crystallographic data of **1** in CIF format and details of synthesis, characterization, and fluorescence quenching studies. This material is available free of charge via the Internet at <http://pubs.acs.org>.

■ AUTHOR INFORMATION

Corresponding Author

*E-mail: psm@ipc.iisc.ernet.in. Tel: 91-80-22933352. Fax: 91-80-23601552.

Notes

The authors declare no competing financial interest.

■ ACKNOWLEDGMENTS

The authors are grateful to CSIR-Delhi and STC-IISc for financial support and Johnson Matthey Pvt. Ltd. U.K. for the generous supply of K₂PtCl₄ as a loan.

■ REFERENCES

- (1) (a) Stang, P. J.; Olenyuk, B. *Acc. Chem. Res.* **1997**, *30*, 502. (b) Chakrabarty, R.; Mukherjee, P. S.; Stang, P. J. *Chem. Rev.* **2011**, *111*, 6810. (c) Xu, X.; Nieuwenhuyzen, M.; James, S. L. *Angew. Chem., Int. Ed.* **2002**, *41*, 764.
- (2) (a) Fujita, M. *Chem. Soc. Rev.* **1998**, *27*, 417. (b) De, S.; Mahata, K.; Schmittl, M. *Chem. Soc. Rev.* **2010**, *39*, 1555.
- (3) Breiner, B.; Clegg, J. K.; Nitschke, J. R. *Chem. Sci.* **2011**, *2*, 51.
- (4) (a) Wang, M.; Zheng, Y. R.; Cook, T. R.; Stang, P. J. *Inorg. Chem.* **2011**, *50*, 6107. (b) Wang, M.; Zheng, Y. R.; Ghosh, K.; Stang, P. J. *J. Am. Chem. Soc.* **2010**, *132*, 6282.
- (5) (a) Chand, D. K.; Biradha, K.; Fujita, M. *Chem. Commun.* **2001**, 1652. (b) Therrien, B. *Eur. J. Inorg. Chem.* **2009**, 2445. (c) Han, Y.-F.; Jia, W.-G.; Yu, W.-B.; Jin, G.-X. *Chem. Soc. Rev.* **2009**, *38*, 3419. (d) Shanmugaraju, S.; Samanta, D.; Mukherjee, P. S. *Beilstein J. Org. Chem.* **2012**, *8*, 313. (e) Mirtschin, S.; Slabon-Turski, A.; Scopelliti, R.; Velders, A. H.; Severin, K. *J. Am. Chem. Soc.* **2010**, *132*, 14004.
- (6) (a) McQuade, D. T.; Pullen, A. E.; Swager, T. M. *Chem. Rev.* **2000**, *100*, 2537. (b) Toal, S. J.; Trogler, W. C. *J. Mater. Chem.* **2006**, *16*, 2871. (c) Germain, M. E.; Knapp, M. J. *Chem. Soc. Rev.* **2009**, *38*, 2543.
- (7) Moore, D. S. *Rev. Sci. Instrum.* **2004**, *75*, 2499.
- (8) (a) Ghosh, S.; Mukherjee, P. S. *Organometallics* **2008**, *27*, 316. (b) Shanmugaraju, S.; Joshi, S. A.; Mukherjee, P. S. *Inorg. Chem.* **2011**, *50*, 11736. (c) Qin, Z.; Jennings, M. C.; Puddephatt, R. J. *Inorg. Chem.* **2003**, *49*, 1956.
- (9) (a) Fant, F.; de Sloovere, A.; Matthijssen, K.; Marle, C.; Fantroussi, V.; Verstraete, W. *Environmental Pollution*; Elsevier: Oxford, U.K., 2000; Vol. *111*, p 503. (b) Lee, Y.-H.; Liu, H.; Lee, J.-Y.; Kim, S.-H.; Kim, S.-K.; Sessler, J. L.; Kim, Y.; Kim, J.-S. *Chem.—Eur. J.* **2010**, *16*, 5895.